Magnesium Technology 2012
Edited by: Suveen N. Mathaudhu, Wim H. Sillekens, Neale R. Neelameggham, and Norbert Hort
TMS (The Minerals, Metals & Materials Society), 2012

EFFECT OF THICKNESS ON THE MORPHOLOGY AND CORROSION BEHAVIOR OF CERIUM-BASED CONVERSION COATINGS ON AZ31B MAGNESIUM ALLOY

Carlos E. Castano[1], Surender Maddela[1], Matthew J. O'Keefe[1], Yar-Ming Wang[2]
[1] Materials Research Center, Department of Materials Science and Engineering, Missouri University of Science and Technology; 305 McNutt Hall 1400N Bishop; Rolla, MO, 65409, USA
[2]Chemical Sciences and Materials Systems Laboratory, GM R&D Center; MC: 480-106-224, 30500 Mound Rd; Warren, MI 48090-9055, USA

Keywords: Cerium-based Conversion Coatings, Corrosion of Magnesium Alloys, Transmission Electron Microscopy, Coating Thickness.

Abstract

Cerium-based conversion coatings (CeCCs) were deposited onto AZ31B magnesium alloy substrates using a spontaneous reaction of $CeCl_3$, H_2O_2 and gelatin in a water-based solution. The coating thickness was adjusted by controlling the immersion time in the deposition solution. Prior to deposition, the AZ31B substrates were treated using an acid pickling in nitric acid and then an alkaline cleaning in sodium metasilicate pentahydrate. After deposition, the coated samples were immersed in a phosphate bath that converted cerium oxide/hydroxide into cerium phosphate. Electrochemical impedance spectroscopy, potentiodynamic polarization and neutral salt spray testing studies indicated that ~100 nm thick CeCC had better corrosion performance than ~400 nm coatings. Characterization of the CeCCs by transmission electron microscopy (TEM) revealed a three layer structure with different compositions.

Introduction

Recently there has been increased interest in using magnesium-based alloys in a number of applications. The main motivation for this interest is that magnesium alloys offer a high potential for use as a lightweight structural material for automotive and aerospace components [1-4]. Comparing the densities of Mg (1.74 g/cm^3), Al (2.70 g/cm^3) and Fe (7.84 g/cm^3), magnesium is 35% lighter than aluminum and 77% lighter than iron [1]. However, the use of magnesium and its alloys in the automotive industry is limited due to poor corrosion performance [1,2]. Magnesium AZ91 alloy is one of the most commonly used alloys in the automotive industry due to its relatively low cost, good yield strength, and acceptable corrosion resistance. However, the amount of Al (~ 9wt %) in AZ91 reduces ductility due to the formation of brittle second phases [5,6]. In contrast, Mg AZ31 alloy is one of the most promising alloys for automobile applications because it offers a good combination of strength and ductility [6]. Nevertheless, the corrosion resistance of AZ31 alloy is still a great concern. Corrosion resistance of magnesium alloys can be increased by the use of conversion coatings that not only provide a barrier between the substrate and its environment but also supply a suitable substrate for paint coatings. Rare earths conversion coatings, principally CeCCs, have demonstrated improvements on the corrosion resistance for magnesium alloys [7-10]. CeCCs are commonly considered to be environmentally friendly corrosion inhibitors on aluminum alloys. Nevertheless, the effectiveness of the CeCCs on the corrosion protection has been highly dependent on surface pretreatment, deposition parameters and post-treatment [2, 7-10]. Current progress at the Missouri University of Science and Technology has developed an adequate surface pretreatment for deposition of CeCCs on AZ91D magnesium alloy consisting of acid then alkaline cleaning that can be applied to other magnesium alloys [8]. In this study, an optimization was carried out to correlate thickness, microstructure, and deposition time of cerium conversion coatings with the corrosion performance of Mg AZ31B alloy.

Experimental Procedure

Cerium conversion coatings were deposited onto Mg AZ31B alloy coupons of dimensions 100 mm x 50 mm x 2 mm. Prior to deposition, AZ31B alloy panels were mechanically polished using 180 grit abrasive SiC papers, then cleaned with isopropyl, rinsed with deionized water, and finally dried in air at room temperature. The surface of the cleaned samples was pretreated in 1 wt% nitric acid aqueous solution for 30 seconds followed by an alkaline cleaning in 5 wt% of $Na_2SiO_3{\cdot}5H_2O$ aqueous solution for 5 minutes at room temperature. The CeCC aqueous solution consisted of 4 wt% of $CeCl_3{\cdot}7H_2O$ (99.9 %, Alfa Aesar), 6.7 wt% of hydrogen peroxide (Fisher Chemical, 30 vol%), and 0.25 wt% of organic gelatin (RDH, Rousselot) in DI water. Mg AZ31B alloy coupons were immersed in the CeCC solution for 5 s, 60 s, 120 s, and 180 s to produce various layer thicknesses. Finally, coated samples were postreated for 5 min at 85 °C in a 2.5 wt% NaH_2PO_4 aqueous solution to convert the coating into $CePO_4$ [11]. Electrochemical measurements were carried out in 1.6 wt% NaCl solution using a flat cell of 1 cm^2 of exposed area (model K0235, Princeton Applied Research) with a saturated calomel electrode (SCE) and platinum mesh served as a reference and counter electrodes, respectively. Open circuit potential (OCP) was monitored for 1000 seconds before impedance and potentiodynamic polarization measurements. The cyclic potentiodynamic scans were conducted from -0.3 to +0.8 V and scanned back to -0.25 V with a scan rate of 1 mV/s with respect to OCP using an EG&G potentiostat model 273A (Princeton Applied Research). Corrware software was used to control the analytical equipment and CView and ZView were used for data fitting analysis. The corrosion performance of the coated panels was also evaluated by ASTM B117 neutral salt fog testing. Electrochemical impedance spectroscopy (EIS) was performed using a Schlumberger model SI1255 frequency response analyzer in combination with the above-mentioned potentiostat. Data were collected over a frequency range of 0.01 to 1x10^5 Hz with 10 mV AC with five points per decade. The TEM samples were prepared using the Helios NanoLab 600. The dual beam system is equipped with a focused ion beam (FIB) milling system that was used in conjunction with a micromanipulator to mount ~100 nm thick TEM specimens onto Cu grids for subsequent TEM characterization.

Results and Discussion

A cross-sectional TEM image of a representative microstructure of an as-deposited CeCC on a AZ31B alloy substrate is shown in Figure 1. A three layer coating structure was identified. Initially, a transition layer shows a porous structure and the cerium conversion coating can be divided in two sublayers 1 and 2. From Figure 2 the structure of sublayer 1 revealed a nanocrystalline region of the CeCC and the thickness is approximately constant over the entire sample, whereas the structure of sublayer 2 is practically amorphous and the thickness varies.

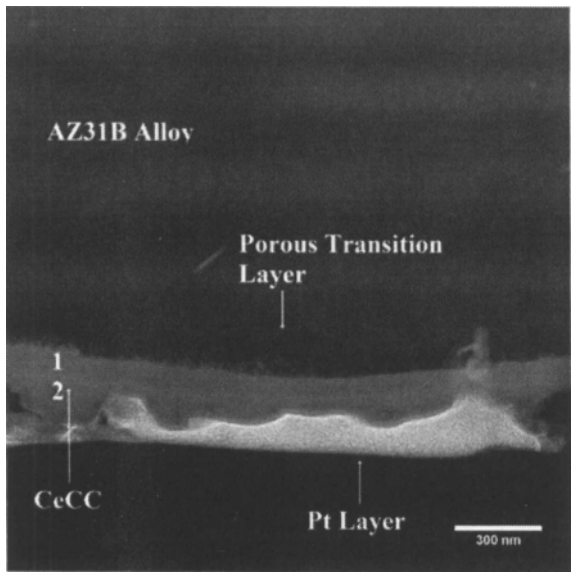

Figure 1. Cross-sectional STEM micrograph showing the microstructure of the 5s immersion sample.

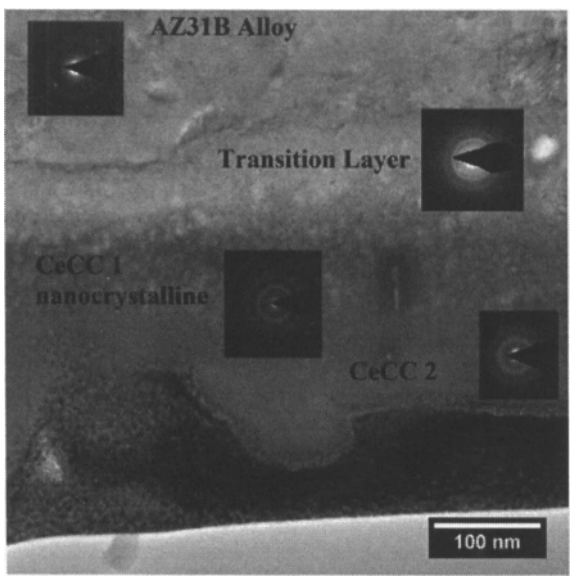

Figure 2. Cross-sectional bright field TEM micrograph of CeCC on AZ31B and corresponding SAD patterns of the different regions.

Chemical analysis by energy dispersive spectroscopy (EDS) revealed that the porous transition layer is composed of Mg, Al, O and C. In addition, EDS on the different sublayers of the CeCC revealed that the conversion coating consisted predominately of Ce, P, and O but the concentration of P throughout the entire thickness of sublayer 2 was higher than in sublayer 1. Based on TEM analysis, the variation of the average thickness of the transition layer, the CeCC coating (sublayer 1 + 2) and the total thickness (transition layer + CeCC coating) with different immersion times are presented in Figure 3. From the analysis, the thickness increased with immersion time except for the 180 s deposition.

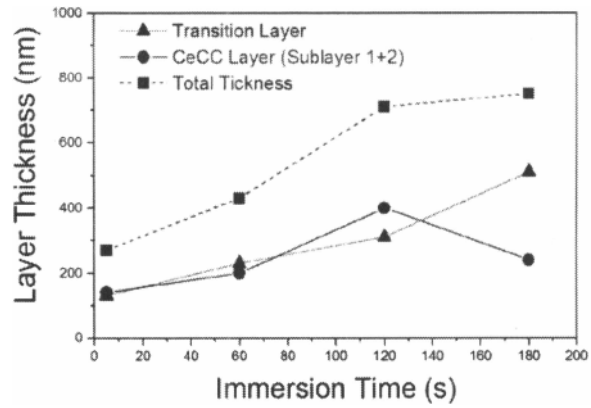

Figure 3. Coating layer thickness as a function of immersion time.

Selective area diffraction patterns from different regions of a representative coated panel are shown in Figure 4.

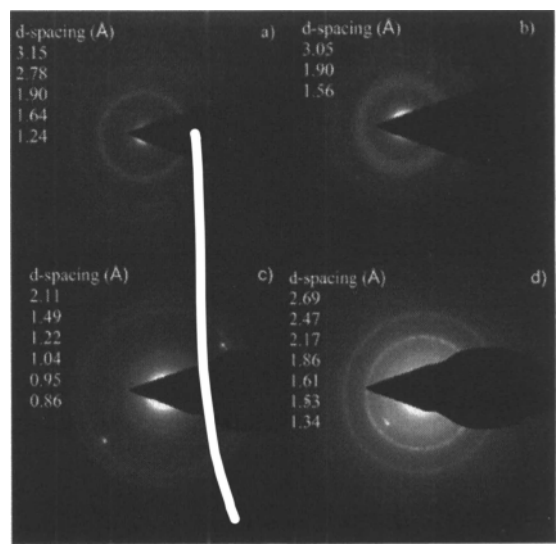

Figure 4. Electron diffraction patterns (SAD) of CeCC on AZ31B from different regions: a) sublayer 1, b) sublayer 2, c) transition layer, and d) AZ31B alloy.

Figures 4 a) and b) show the selected area diffraction patterns (SAD) of the cerium conversion coating. A nanocrystalline structure is suggested since the SAD pattern contained continuous rings. However, a few diffused halos on the pattern showed in

Figure 4 b) are consisted with a structure that is largely amorphous. From Figure 4 a) the rings of the SAD pattern correspond to CeO_2 (PDF 00-034-0394).
The electron diffraction pattern collected from the interfacial region would indicated a nanocrystalline structure, and the pattern can be indexed to MgO (PDF 00-045-0946), Figure 4 c.
Figure 4 d) shows the rings and spots of the electron diffraction micrograph, which is identified as hexagonal Mg (PDF 00-035-0821). Summary of measurements performed on the diffraction patterns is presented in Table I.

TABLE I. d-spacing (Å) calculated from SAD patterns of the different regions and .

CeCC 1	CeCC 2	*CeO_2 PDF 00-034-0394	Transition Layer	*MgO PDF 00-045-0946	AZ31B Alloy	*Mg PDF 00-035-0821
3.15	3.05	3.12		2.43	2.69	2.61
2.78		2.71	2.11	2.11	2.47	2.45
1.90	1.90	1.91	1.49	1.49	2.17	
1.64		1.63	1.22	1.22	1.86	1.90
	1.56	1.56	1.04	1.05	1.61	1.61
1.24		1.24	0.95	0.97	1.53	1.47
			0.86	0.86	1.34	1.37

**Taken from International Centre for Diffraction Data, PDF 4+*

Optical images of the CeCCs obtained at different immersion times after 5 days of salt spray testing are compared to as coated samples in Figure 5. Corroded panels revealed that 5s of immersion in cerium solutions had better corrosion resistance compared to longer immersion times. The panel coated during an 180 s in immersion had numerous pits and salt tails after testing. Although all samples had visible corrosion product after 5 days in salt fog test, the 5s immersion sample exhibited only filiform corrosion while the 60 s, 120 s, and 180 s immersion samples had filiform and pitting corrosion.

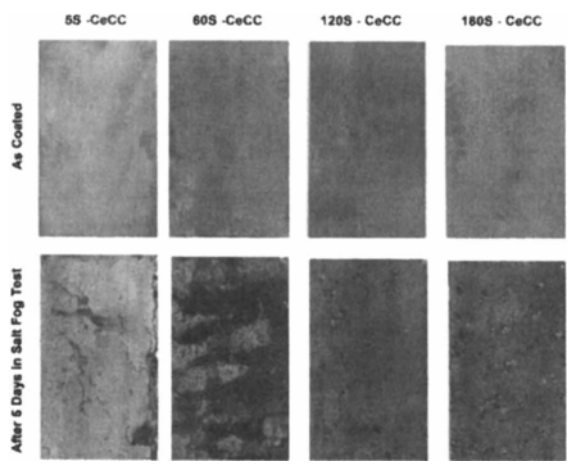

Figure 5. Optical images of cerium conversion coatings on AZ31B Mg alloy at different immersion time before and after 5 days of salt spray testing.

Cyclic potentiodynamic curves of bare and coated AZ31B samples at different immersion times are presented in Figure 6. The corrosion parameters calculated from cyclic potentiodynamic polarization curves are presented in Table II.

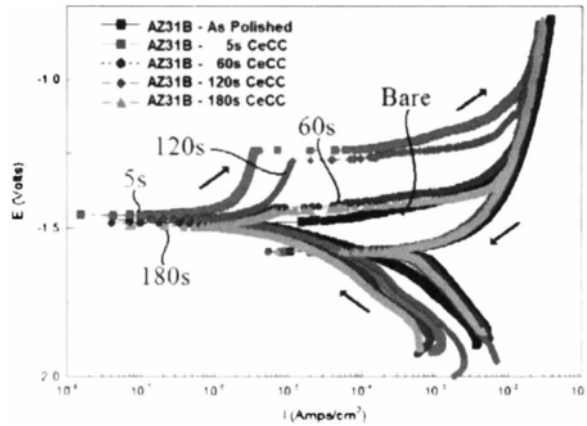

Figure 6. Cyclic potentiodynamic polarization behavior of cerium conversion coatings on AZ31B alloy at different deposition times

The corrosion potential (E_{corr}) of AZ31B panels with a CeCC is basically the same value as was obtained for bare samples (as polished). The reverse scans for all measured samples, Figure 6, have a more active potential than the free corrosion potential. This implies a high probability of localized corrosion of the AZ31B alloy even with a conversion coating [7]. However, the corrosion resistance increased for coated samples because the CeCC increases the pitting potential. In particular, an appreciable anodic passivation region (~220 mV) for AZ31B after 5s in immersion is evident in Figure 6. Although a limited passivation region is measured for 60 s and 180 s immersion panels, the pitting potential increased only ~40mV. As a result, it is expected that the specimen will undergo pitting attack once the free corrosion potential is reached. The corrosion current densities (i_{corr}) of CeCC samples are significantly reduced compared to the bare sample and the lowest i_{corr} was obtained for the 5s immersion time panel. Calculated values of corrosion rate are directly proportional to the immersion time, which is also directly proportional to the coating thickness.

TABLE II. Corrosion parameters derived from the potentiodynamic polarization experiments.

Sample AZ31B	βa mv/dec	βc mv/dec	i_{corr} μA/cm²	E_{corr} mV_{SCE}	E_{pit} mV	Corr. Rate mm/y
As Polished	20	-68	5.0	-1490	-1490	0.11
5S CeCC	149	-57	0.8	-1460	-1240	0.02
60S CeCC	75	-50	1.5	-1480	-1430	0.03
120S CeCC	133	-47	1.8	-1480	-1270	0.04
180S CeCC	87	-79	2.2	-1490	-1450	0.05

Impedance spectroscopy results from coated and uncoated samples are shown in Figure 7. The recorded spectra of the bare sample exhibited one capacitive loop and coated samples displayed two capacitive loops. This indicates that coated samples can be modeled by an electrical equivalent circuit that represents a coated alloy with a defect and the bare sample with a simple Randal's model, as shown Figure 8.

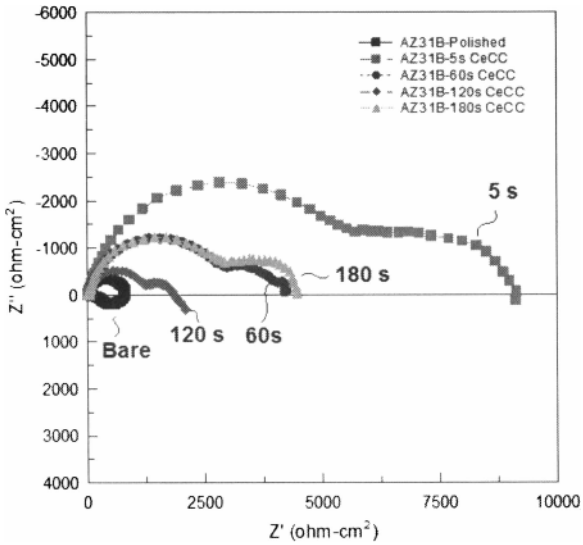

Figure 7. Impedance spectra of cerium conversion coatings on AZ31B alloy at different deposition times.

In figure 8, R_s is the solution resistance, R_p is the coating defect resistance, R_{ct} is the polarization resistance or charge-transfer resistance at the metal interface. The symbols Q_{ox} and Q_{dl} are two constant phase elements used to represent the non-ideal coating capacitance and the double layer capacitance, where n_{ox} and n_{dl} are equal to 1 for an ideal capacitor and less than 1 for non-uniform surfaces. The inductance is labeled L and represents the formation of a surface layer [8].

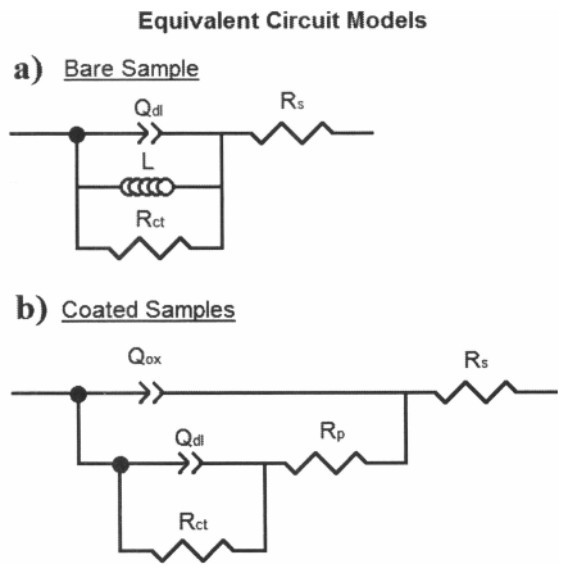

Figure 8. Equivalent circuit models used to fit impedance data: a) simple Randal's model with inductive loop for bare sample and b) two time constant model for cerium coated Mg AZ31B alloy.

The equivalent circuits have been utilized to fit the electrochemical data obtained from bare and cerium-based coated AZ31B panels and the results are summarized in Table III. The 5s CeCC sample had the maximum polarization resistance (5923 Ω cm^2) and the highest defect or pore resistance (2921 Ω cm^2). Additionally, comparing coated panels the 5s sample has the lowest Q_{dl} value, indicating a lower amount of area that is corroding [9].

TABLE III. Corrosion parameters derived from the potentiodynamic polarization experiments.

Sample AZ31B	As Polished	5S CeCC	60S CeCC	120S CeCC	120S CeCC
Rs $\Omega \cdot cm^2$	20	32	25	29	29
Qox $\Omega^{-1} \cdot s^n \cdot cm^{-2}$		9.12×10^{-6}	1.39×10^{-5}	1.33×10^{-5}	1.62×10^{-5}
n_{ox}		0.87	0.86	0.89	0.89
Qdl $\Omega^{-1} \cdot s^n \cdot cm^{-2}$	1.13×10^{-5}	5.36×10^{-4}	1.10×10^{-3}	1.52×10^{-3}	9.11×10^{-4}
n_{ox}	0.94	0.92	0.90	0.87	0.82
Rct $\Omega \cdot cm^2$	799	2921	1159	641	1626
Rp $\Omega \cdot cm^2$		5923	3009	1232	2928
L $\Omega^{-1} \cdot \sqrt{s}/cm^2$	873				

In general the electrochemical results are consistent with the performance observed in salt spray testing. Both electrochemical and salt spray cabinet results indicated that ~100 nm thick cerium-based conversion coatings deposited by 5s immersion provide the best corrosion resistance on Mg AZ31B alloy substrates.

Conclusions

The effect of immersion time on the morphology, thickness and corrosion behavior of cerium-based conversion coatings on magnesium AZ31B alloy was investigated. The as-deposited coatings system consisted of a three layer structure: (1) a nanocrystalline MgO transition layer in contact with the Mg substrate, (2) a nanocrystalline CeCC layer, and (3) an outer amorphous CeCC layer. The nanocrystalline CeCC layer thickness was a function of immersion time in the deposition solution and ranged from a minimum of ~100 nm (5s immersion) to a maximum of ~400 nm (120s immersion). In general, at all thicknesses the cerium-based conversion coatings improve the corrosion resistance of AZ31B magnesium in chloride media. However, the corrosion resistance of AZ31B magnesium alloy was best for thinner CeCCs. Based on the correlation of deposition time and corrosion behavior, layers of ~100 nm thick obtained by immersion for ~ 5s exhibited a ~5.5X improvement in corrosion resistance vs. bare, as-polished panels. The presence of fewer and smaller cracks in 5s immersion panels, and larger cracks in panels coated at the longer times, provide some explanation for the improved corrosion performance.

Acknowledgements

The authors would like to extend their thanks to the USAMP team: Adam Stals, Jim Quinn, Kevin Cunningham and Harry Kuo. They also appreciate the technical assistance of Dr. Beth Kulp (FIB/SEM) and Dr. Kai Song (TEM) of the Materials Research Center at the Missouri University of Science and Technology.
This material is based upon work supported by the Department of Energy National Energy Technology Laboratory under Award

Numbers DE-FC26-02OR22910 and DE-EE0003583. This report was prepared as an account of work sponsored by an agency of the United States Government. Neither the United States Government nor any agency thereof, nor any of their employees, makes any warranty, express or implied, or assumes any legal liability or responsibility for the accuracy, completeness, or usefulness of any information, apparatus, product, or process disclosed, or represents that its use would not infringe privately owned rights. Reference herein to any specific commercial product, process, or service by trade name, trademark, manufacturer, or otherwise does not necessarily constitute or imply its endorsement, recommendation, or favoring by the United States Government or any agency thereof. The views and opinions of authors expressed herein do not necessarily state or reflect those of the United States Government or any agency thereof.

References

1. Friedrich H. E. Mordike B.L. *Magnesium Technology: Metallurgy, Design data, Applications*. Springer – Verlag Berlin Heidelberg (2006).
2. M. K. Kulekci, "Magnesium and its Alloys Applications in Automotive Industry," *The International Journal of Advanced Manufacturing Technology*. 39 (9-10) 851–865 (2008).
3. G. L. Song, A. Atrens, "Corrosion Mechanisms of Magnesium Alloys," *Advanced Engineering Materials*, 1(1) 11-33 (1999).
4. G. L. Song, A. Atrens, "Understanding Magnesium Corrosion: a Framework for Improved Alloy Performance," *Advanced Engineering Materials*, 5(12) 837-858 (2003).
5. E. Ghali, W. Dietzel and K. U. Kainer, "General and Localized Corrosion of Magnesium Alloys: A Critical Review," *Journal of Materials Engineering and Performance*, 13, 7-23 (2004).
6. M. Marya et al., "Microstructural Effects of AZ31 Magnesium Alloy on its Tensile Deformation and Failure Behaviors," *Materials Science and Engineering A*, 418, 341-356 (2006).
7. M. Dabalà, K. Brunelli, E. Napolitani, M. Magrini. "Cerium-based Chemical Conversion Coatings on AZ63 Magnesium Alloy." *Surface and Coatings Technology*, 172 227-232 (2003).
8. S. Maddela, M. J. O'Keefe, Y. -M. Wang, H. -H. Kuo. "Influence of Surface Pretreatment on Coating Morphology and Corrosion Performance of Cerium-Based Conversion Coatings on AZ91 D Alloy." *Corrosion*, 66(11) 115006-1/115006-8 (2010).
9. K. Brunelli, M. Dabalà, I. Calliari, M. Magrini. "Effect of HCl Pre-treatment on Corrosion Resistance of Cerium-based Conversion Coatings on Magnesium and Magnesium alloys." *Corrosion Science*, 47(4) 989-1000 (2005).
10. A. L. Rudd, C. B. Breslin, F, Mansfeld. "The Corrosion Protection Afferded by Rare Earth Conversion Coatings Applied to Magnesium." *Corrosion Science*, 42 275-288 (2000).
11. D. K. Heller, W. G. Fahrenholtz, M. J. O'Keefe, "The Effect of Post-treatment Time and Temperature on Cerium-based Conversion Coatings on Al 2024-T3," *Corrosion Science*, 52(2) 360-368 (2010).